Dynamic Systems and Applications 32 (2023) 18-32

NONLINEAR RESPONSE OF A POSITION DEPENDENT MASS SYSTEM DRIVEN BY AN AMPLITUDE MODULATED FORCE

K. SUDDALAI KANNAN[1], S.M. ABDUL KADER[1],
M.V. SETHUMEENAKSHI[2],V. CHINNATHAMBI[1,*], S. RAJASEKAR[3]

[1]Department of Physics, Sadakathullah Appa College, Tirunelveli-627 011, Tamilnadu, India
[2]Department of Mathematics, Fatima College, Madurai-625 018, Tamilnadu, India.
[3]School of Physics, Bharathidasan University, Tiruchirapalli 620 024, Tamilnadu, India.
[*]Corresponding author Email: veerchinnathambi@gmail.com

ABSTRACT. This paper highlights on the occurrence of vibrational resonance (VR), investigated in a double-well position-dependent mass (PDM)-Duffing oscillator system driven by an amplitude modulated (AM) force. The AM force consists of one low-frequency (ω) component and two high-frequencies ($\Omega + \omega$) and ($\Omega - \omega$) components with ($\Omega \gg \omega$). In the PDM-Duffing oscillator with one low-frequency and one high-frequency forces, by applying a theoretical approach an analytical expression is obtained for the response amplitude at the low-frequency (ω). The system provides an interesting scenario where PDM function makes a significant contribution to the occurrence of VR. We examine the role played by PDM parameters (m_0, λ) and force parameters (g, ω, Ω) on VR. We show the enhanced response amplitude Q at the low-frequency ω, showing more number of resonance peaks, a non-decay of response amplitude and hysteresis and a jump phenomenon on the response amplitude curve due to the amplitude modulated force. Results of analytical investigations are validated and complemented by numerical simulation.

AMS (MOS) Subject Classification. 34K18, 37C29, 65P20, 65P30, 74H65.

Key Words and Phrases. Position dependent mass system, Amplitude modulated force, Vibrational resonance, Hysteresis, Chaos.

1. INTRODUCTION

Vibrational resonance (VR) was first reported by Landa and McClintock [1] in biharmonically driven bistable systems when there is a large difference between the frequencies ($\Omega \gg \omega$) of the two driving forces. Thereafter, an analytical investigation

Received January 19, 2023 ISSN 1056-2176(Print); ISSN 2693-5295 (online)
www.dynamicpublishers.org https://doi.org/10.46719/dsa2023.32.02

to confirm VR was carried out by Gitterman [2]. After these investigations, the features of VR have been studied theoretically, numerically and experimentally in a variety of nonlinear systems [3–15]. The mass changes with respect to either velocity or position, time or both position and time is known as varying mass. The position-dependent mass (PDM) approach has a wide range of applications in various areas of science [16–20]. A very notable application of the field is in the micro-fabrication technique which includes molecular-beam epitaxy and nanolithography [21–23]. This paper investigates, the position-dependent mass (PDM) system, which is position-dependent mass-Duffing oscillator under the influence of an amplitude modulated force.

This paper is structured into five sections. To get initiated with, at first we introduced the position-dependent mass-Duffing oscillator system in Sec.2. The system was treated with only one high-frequency force which is explained in Sec.3. We obtain the equation of motion and an approximate analytical expression for the response amplitude Q of the low-frequency output oscillation. This analytical expression of Q is used to analyze the occurrence of VR and verify the theoretical predictions through numerical simulation. We take up the system with two high-frequency forces in Sec.4. By numerical technique, we show the occurrence of enhanced VR, hysteresis and a jump phenomenon and various dynamical behaviours in the PDM system. Section 5 deals with the conclusion of the research.

2. **Position Dependent Mass-Duffing Oscillator**

The Lagrangian L is defined as $L = T - V$, where T is the kinetic energy and V the potential energy of the system. The Lagrangian function of a classical oscillator is given by

$$L(x, \dot{x}, t) = T - V(x) = \frac{1}{2} m(x)\dot{x}^2 - V(x) \tag{2.1}$$

and the associated Lagrangian equation of motion with external contributions (Φ) to the motion of the system can be written as

$$\frac{d}{dt}\left(\frac{\partial L}{\partial \dot{x}}\right) - \left(\frac{\partial L}{\partial x}\right) = \Phi \tag{2.2}$$

Using the Lagrangian function (Eq.2.1) in the Euler-Lagrangian equation (Eq.2.2), the corresponding equation of motion of classical oscillator can be written as

$$m(x)\ddot{x} + \frac{1}{2} m'(x)\dot{x}^2 + \frac{dV(x)}{dx} = \Phi, \tag{2.3}$$

where Φ is the external contributions to the motion from dissipative and driving force ($F(t)$). The external driving force assumed here to be AM force. The analytical expression for AM force is $F(t) = (f + 2g\cos\Omega t)\sin\omega t$ with $\Omega >> \omega$. Hence the external contributions to the motion $\Phi = -\alpha\dot{x} + F(t)$, where α is the damping

coefficient, f and ω are the amplitude and frequency of the low-frequency component and g and Ω are the amplitude and frequency of the high-frequency component of the AM force. The prime in Eq.(2.3) implies differentiation with respect to space variable x and the overdot indicates differentiation with respect to time. In the present work, we consider a Duffing type oscillator potential

$$V(x) = \frac{1}{2}\, m(x)\, \omega_0^2\, x^2 + \frac{1}{4}\, \beta\, x^4\ , \tag{2.4}$$

where ω_0 is the oscillator's natural frequency and β is the stiffness constant which plays the role of the nonlinear parameter. The following mass function is used in the present study.

$$m(x) = \frac{m_0}{1 + \lambda x^2}\ , \tag{2.5}$$

where $m(x)$ is a variable mass with position, m_0 is a constant mass, equivalent to the mass amplitude and λ is the strength of the spatial nonlinearity in mass. This mass function was first proposed by Mathews and Lakshmanan [24] in relation to relativistic fields of elementary particles and it appears frequently in the modelling of diverse nonlinear mechanical systems [25, 26]. Recently, using this mass function, Roy-Layinde et al. [27] examined and analyzed the VR phenomenon in double-well PDM-Duffing oscillator system driven by biharmonic force. In the present work, we analyze both analytically and numerically the occurrence of VR in double-well PDM-Duffing oscillator system driven by an AM force. From the above one can easily show that the equation of motion of the PDM-Duffing oscillator can be written as

$$m(x)\ \ddot{x} - m^2(x)x\gamma\lambda\dot{x}^2 + \alpha\dot{x} + m^2(x)\gamma\ \omega_0^2\ x + \beta x^3 = (f + 2g\cos\Omega t)\sin\omega t,\ \ \Omega >> \omega. \tag{2.6}$$

With the use of the formula $2\cos\Omega t\sin\omega t = \sin(\Omega+\omega)t + \sin(\Omega-\omega)t$, we arrive at Eq.(2.6),

$$\begin{aligned} &m(x)\ \ddot{x} - m^2(x)x\gamma\lambda\dot{x}^2 + \alpha\dot{x} + m^2(x)\gamma\ \omega_0^2\ x + \beta x^3 = \\ &\quad f\sin\omega t + g\sin(\Omega+\omega)t + g\sin(\Omega-\omega)t,\ \ \Omega >> \omega. \end{aligned} \tag{2.7}$$

where $\gamma = \frac{1}{m_0}$. For a unit mass amplitude, ($m_0 = 1$) and negligible strength of nonlinearity in mass, ($\lambda = 0$), Eq.(2.7) reduces to the well known Duffing oscillator driven by an AM force. The physical system (Eq.2.7) describes a dual frequency driven gas bubble in which the mass of the bubble is dependent on the bubble's radius, which is a spatial coordinate [27, 28]. In order to find the solution of Eq.(2.7), we use the method of direct separation of motions (MDSM) described by Blekhman [29] as it is the most effective formulation of vibrational mechanics to obtain the equation of motion of the slow motion which can be modulated by parameters of the fast driving force analytically. Eq.(2.7) can not fit into the general framework of

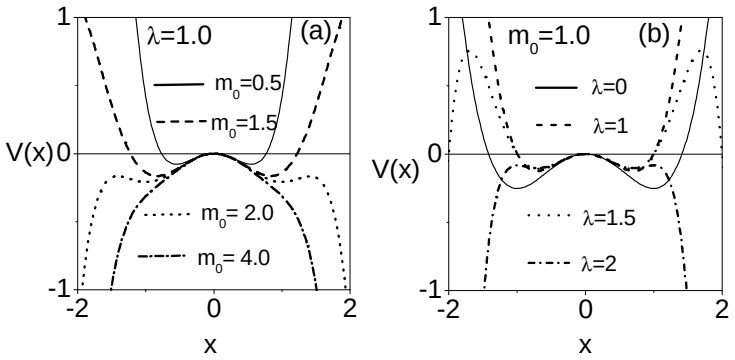

FIGURE 1. Shape of the potential $V(x)$ for (a) $\lambda = 1.0, m_0 = 0.5, 1.5, 2.0, 4.0$ (b) $m_0 = 1.0, \lambda = 0, 1.0, 1.5, 2.0$. The values of the other parameters are $\beta = 1$ and $\omega_0^2 = -1$.

MDSM. By suitable approximations as given in the ref.[27], the following equation of motion can be used to apply the MDSM method,

$$\ddot{x} - \lambda(x - \lambda x^3 + \lambda^2 x^5)\dot{x}^2 + \alpha\gamma(1 + \lambda x^2)\dot{x} + \omega_0^2 x + \delta x^3 + \xi x^5 = \gamma(1 + \lambda x^2)\,(f\sin\omega t + g\sin(\Omega + \omega)t + g\sin(\Omega - \omega)t), \quad \Omega >> \omega. \tag{2.8}$$

where $\delta = \beta\gamma - \lambda\omega_0^2$ and $\xi = \beta\gamma\lambda + \lambda^2\omega_0^2$. Eq.(2.8) is also known as the PDM-Duffing oscillator equation. The corresponding potential of the system is

$$V(x) = \frac{\omega_0^2}{2}\, x^2 + \frac{\delta}{4}\, x^4 \; + \frac{\xi}{6}\, x^6 \; . \tag{2.9}$$

In this study, we choose the mass parameter regimes within which the system potential is double-well, so that $0 < m_0 < 1.5$ and $0 < \lambda < 1$ for $\alpha = 0.2, \omega_0^2 = -1, \beta = 1$ and $f = 0.05$. The system potential shown in Figs.1(a) and 1(b) for different values of the PDM parameters of the mass amplitude $m_0 (= 0.5, 1.5, 2.0, 4.0)$ with $\lambda = 1.0$ and the strength of the spatial nonlinearity in mass $\lambda = (0, 1.0, 1.5, 2.0)$ with $m_0 = 1.0$, is computed from Eq.(2.9).

3. **PDM-Duffing Oscillator with One High-Frequency Force**

When $\Omega \gg \omega$, the AM force can be treated as consisting of a low-frequency force $f\sin\omega t$ and two high-frequency forces, such as $g\sin(\Omega+\omega)t$ and $g\sin(\Omega-\omega)t$. Firstly we observed the system with the external force consisting of one low-frequency force $f\sin\omega t$ and one high-frequency force $g\sin(\Omega + \omega)t$, then the equation of the system is expressed by

$$\ddot{x} - \lambda(x - \lambda x^3 + \lambda^2 x^5)\dot{x}^2 + d\gamma(1 + \lambda x^2)\dot{x} + \omega_0^2 x + \delta x^3 + \xi x^5 = \gamma(1 + \lambda x^2)\,(f\sin\omega t + g\sin(\Omega + \omega)t), \quad \Omega >> \omega. \tag{3.1}$$

We observed the VR realized with this force through a theoretical approach. We arrived at an analytical expression for the response amplitude Q and the value of

the control parameter g at which VR occurs and verify these theoretical predictions through numerical simulation. Then we take up the system with the AM force, to illustrate that the theoretical procedure used to analyze VR in the case of the system with one high-frequency force is not applicable for the system with two high-frequency forces. Hence a numerical investigation for this case is performed.

3.1. **Theoretical Description of VR.** Owing to the presence of two different driving frequencies we expect that the system's response can also been split up into two distinct time scales, one slow and the other fast and accordingly we can write the dynamical variable $X \equiv X(t, \omega t)$ with period $(2\pi/\omega)$ and a fast variable $\psi \equiv \psi(t, \Omega t)$ with period $(2\pi/(\Omega+\omega))$:

$$x(t) = X(t) + \psi(t, \tau). \tag{3.2}$$

The mean value of the fast motion is

$$\overline{\psi} = \frac{1}{2\pi}\int_0^{2\pi} \psi \, \mathrm{d}\tau = 0. \tag{3.3}$$

Due to the rapid varying of ψ, we assume that $\ddot{\psi} \gg \dot{\psi}, \psi, \psi^2, \psi^3, \psi^4$ and ψ^5. This approximation is called as inertial approximation which leads to the equation $\ddot{\psi} = \gamma g \sin(\Omega+\omega)t$ which gives $\dot{\psi} = -\frac{\gamma g}{(\Omega+\omega)}\cos(\Omega+\omega)t$; $\psi = -\frac{\gamma g}{(\Omega+\omega)^2}\sin(\Omega+\omega)t$, $\overline{\psi^2} = \frac{\gamma^2 g^2}{2(\Omega+\omega)^4}$; $\overline{\psi^3} = 0$; $\overline{\psi^4} = \frac{3\gamma^4 g^4}{8(\Omega+\omega)^8}$; $\overline{\dot{\psi}^2} = \frac{\gamma^2 g^2}{2(\Omega+\omega)^2}$ and $\overline{\psi^5} = 0$. When substituting the solution Eq.(3.2) in Eq.(3.1) and using the values of $\overline{\psi}, \overline{\psi^2}, \overline{\psi^3}, \overline{\psi^4}$ and $\overline{\psi^5}$, then the equation for the slow motion is formulated

$$\begin{aligned} \ddot{X} - \lambda(C_1 X + C_2 X^3 + \lambda^2 X^5)\dot{X}^2 + \alpha\gamma(C_3 + \lambda X^2)\dot{X} + \\ \eta_1 X + \eta_2 X^3 + \eta_3 X^5 = \gamma(C_3 + \lambda X^2) f \sin\omega t \end{aligned} \tag{3.4a}$$

where,

$$C_1 = \frac{15\lambda^2\gamma^4 g^4}{8}\left[\frac{1}{(\Omega+\omega)^8}\right] - \frac{3\lambda\gamma^2 g^2}{2}\left[\frac{1}{(\Omega+\omega)^4}\right] + 1 \tag{3.4b}$$

$$C_2 = 5\lambda^2\gamma^2 g^2\left[\frac{1}{(\Omega+\omega)^4}\right] - \lambda, \tag{3.4c}$$

$$C_3 = 1 + \frac{\lambda\gamma^2 g^2}{2}\left[\frac{1}{(\Omega+\omega)^4}\right] \tag{3.4d}$$

$$\begin{aligned} \eta_1 = \frac{\lambda C_1\gamma^2 g^2}{2}\left[\frac{1}{(\Omega+\omega)^2}\right] + \omega_0^2 + \frac{15\xi\gamma^4 g^4}{8}\left[\frac{1}{(\Omega+\omega)^8}\right] + \\ \frac{3\delta\gamma^2 g^2}{2}\left[\frac{1}{(\Omega+\omega)^4}\right] \end{aligned} \tag{3.4e}$$

$$\eta_2 = \frac{\lambda C_2\gamma^2 g^2}{2}\left[\frac{1}{(\Omega+\omega)^2}\right] + 5\xi\gamma^2 g^2\left[\frac{1}{(\Omega+\omega)^4}\right] + \delta \tag{3.4f}$$

$$\eta_3 = \frac{\lambda^3\gamma^2 g^2}{2}\left[\frac{1}{(\Omega+\omega)^2}\right] + \xi \tag{3.4g}$$

and the effective potential is given by,

$$V_{eff}(x) = \frac{\eta_1}{2}X^2 + \frac{\eta_2}{4}X^4 + \frac{\eta_3}{6}X^6 \tag{3.5}$$

The shape, the number of local maxima and minima and their location of the potential $V(x)$ (Eq.2.9) depends on the parameters ω_0^2, δ and ξ but for the effective potential (V_{eff}) (Eq.3.5) these also depend on the force parameters g and Ω. Consequently, by varying g or Ω new equilibrium states can be created whereas the number of equilibrium states can also be reduced. The effective potential of the system (Eq.3.5) is shown in Fig.2(a) for four values of g with $m_0 = 1, \lambda = 0.1$ and in Figure 2(b) for four values of λ with $g = 100, m_0 = 1$. The other parameters values of the system are set as $\omega_0^2 = -1, \beta = 1, \omega = 1.5, \Omega = 15$. In Fig.2(a), V_{eff} is a single-well potential for $g = 0$ and $g = 60$ while it becomes double-well for $g = 100$ and inverted single-well potential for $g = 150$. Similarly in Fig.2(b), V_{eff} is a single-well potential for $\lambda = 0$ and $\lambda = 0.1$ while it becomes a double-well potential for $\lambda = 0.2$ and $\lambda = 0.3$ with $g = 100$ and $m_0 = 1$. The equilibrium points of the oscillations which is slow that

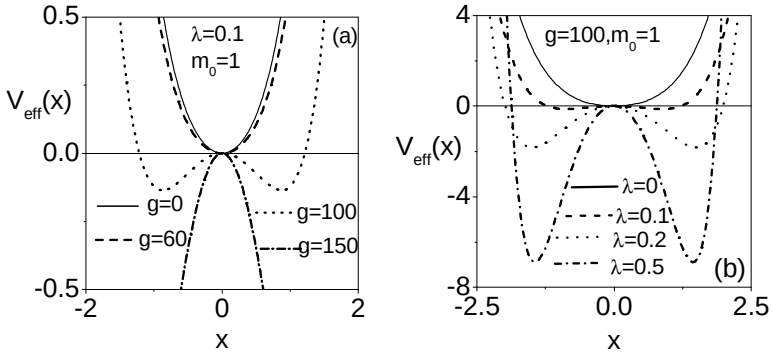

FIGURE 2. The effective potential $V_{eff}(x)$ for (a) $\lambda = 0.1, m_0 = 1.0$ and $g = 0, 50, 100, 150$ (b) $g = 100, m_0 = 1.0$ and $\lambda = 0, 0.1, 0.2, 0.5$. The values of the other parameters are $\beta = 1, f = 0.05, \omega = 1.5, \Omega = 15$ and $\omega_0^2 = -1$.

can be calculated from Eq.(3.4). The equilibrium points of Eq.(3.4) are given by (3.6)

$$X_1^* = 0, \quad X_{2,3}^* = \pm\left[\frac{-\eta_2 + \sqrt{\eta_2^2 - 4\eta_1\eta_3}}{2\eta_3}\right]^{1/2}, \quad X_{4,5}^* = \pm\left[\frac{-\eta_2 - \sqrt{\eta_2^2 - 4\eta_1\eta_3}}{2\eta_3}\right]^{1/2}.$$

Suppose, we choose $\eta_3 > 0$. Then we have the following cases:

Case (i): η_1, $\eta_2 > 0$ or $\eta_1 > 0$, $\eta_2 < 0$ with $\eta_2^2 < 4\eta_1\eta_3$

$X_1^* = 0$ is the only equilibrium point.

Case (ii): $\eta_1 < 0$, η_2-arbitrary

There are three equilibrium points and are X_1^*, $X_{2,3}^*$.

Case (iii): $\eta_1 > 0$, $\eta_2 < 0$ with $\eta_2^2 > 4\eta_1\eta_3$

There are five equilibrium points given by Eq.(3.6).

We obtain the equation for the deviation of the slow motion X from an equilibrium point X^*. Introducing the change of variable $Y = X - X^*$ in Eq.(3.4) we get

$$\ddot{Y} - \lambda(\alpha_1 + \alpha_2 Y + \alpha_3 Y^2 + \alpha_4 Y^3 + \alpha_5 Y^4 + \lambda^2 Y^5)\dot{Y}^2 + \alpha\gamma(\sigma_1 + \sigma_2 Y + \lambda Y^2)\dot{Y}$$
$$+\rho_1 + \rho_2 Y + \rho_3 Y^2 + \rho_4 Y^3 + \rho_5 Y^4 + \eta_3 Y^5 = \gamma(\sigma_1 + \sigma_2 Y + \lambda Y^2) f \sin\omega t \ , \tag{3.7a}$$

where

$$\begin{aligned}
\alpha_1 &= C_1 X^* + C_2 X^{*3} + \lambda^2 X^{*5}, \qquad \alpha_2 = C_1 + 3C_2 X^{*2} + 5\lambda^2 X^{*4} \\
\alpha_3 &= 3C_2 X^* + 10\lambda^2 X^{*2}, \quad \alpha_4 = C_2 + 10\lambda^2 X^{*2} \ , \quad \alpha_5 = 5\lambda^2 X^* \\
\sigma_1 &= C_3 + \lambda X^{*2} \ , \qquad \sigma_2 = 2\lambda X^* \\
\rho_1 &= \eta_1 X^* + \eta_2 X^{*3} + \eta_3 X^{*5} \quad \rho_2 = \eta_1 + 3\eta_2 X^{*2} + 5\eta_3 X^{*4} \\
\rho_3 &= 3\eta_2 X^* + 10\eta_3 X^{*2} \ , \quad \rho_4 = \eta_2 + 10\eta_3 X^{*2} \ , \quad \rho_5 = 5\eta_3 X^*
\end{aligned} \tag{3.7b}$$

For $f \ll 1$ and in the limit $t \to \infty$ we assume that $|Y| \ll 1$ and neglect the nonlinear terms in Eq.(3.7). Then, the solution of linear version of Eq.(3.7) in the limit $t \to \infty$ is $A_{\rm L}\cos(\omega t - \phi)$ where

$$A_{\rm L} = \frac{F}{\left[(\omega_{\rm r}^2 - \omega^2)^2 + \mu^2\omega^2\right]^{1/2}} \ , \tag{3.8}$$

and the resonant frequency is $\omega_{\rm r} = \sqrt{\rho_2}$,$\mu = \alpha\gamma C_3$ and $F = \gamma C_3 f$. When the slow motion takes place around the equilibrium point $X^* = 0$, then $\omega_{\rm r} = \sqrt{\eta_1}$.

The response amplitude Q is

$$Q = \frac{A_{\rm L}}{f} = \frac{\gamma C_3}{\left[(\omega_{\rm r}^2 - \omega^2)^2 + \mu^2\omega^2\right]^{1/2}} \ . \tag{3.9}$$

3.2. **Analysis of Vibrational Resonance.** First we analyze the existence of VR in the system for a particle with constant mass, ie., $m(x) = m_0$ and $\lambda = 0$. We fix the parameters as $\omega_0^2 = -1, \alpha = 0.2, \beta = 1$ and $f = 0.05$. The dependence of the response amplitude Q on the parameters m_0, ω and Ω is illustrated in Fig.3. Along with the increase of these parameters, resonances appear obviously in each plot. Figures 3(a),3(b) and 3(c) show Q versus g for three different values of $m_0 = (0.5, 1.0, 1.4)$ with $\omega = 1.5, \Omega = 15$, Q versus g for four different values of $\omega = (0.75, 1.5, 2.5, 3.0)$ with $m_0 = 0.5, \Omega = 15$ and Q versus g for three different values of $\Omega = (7.5, 21.0, 30.0)$ with $m_0 = 0.5, \omega = 1.5$. Continuous curves represent theoretical result obtained from Eq.(3.9). Solid circles represent numerically calculated Q. From the numerical

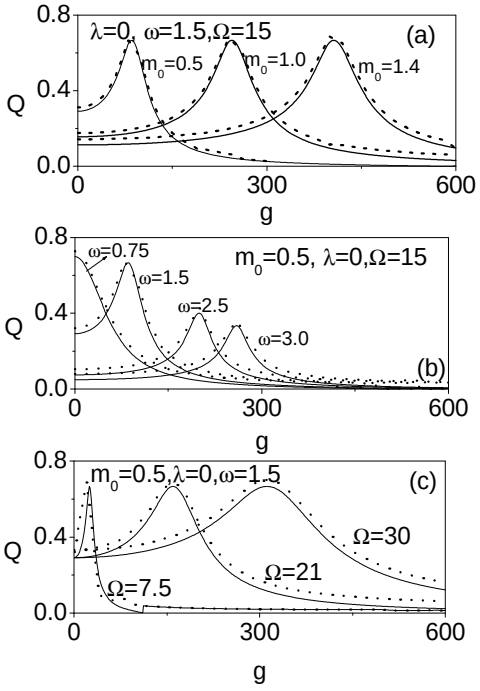

FIGURE 3. The variation of the response amplitude Q with (a) three values of $m_0 = 0.5, 1.0, 1.4$ for $\omega = 1.5, \Omega = 15.0$ (b) four values of $\omega = 0.75, 1.5, 2.5, 3.0$ for $m_0 = 0.5, \Omega = 15.0$ and (c) with g for three values of $\Omega = 7.5, 21, 30$ and $m_0 = 0.5, \omega = 1.5$. The values of the other parameters are $\alpha = 0.2, \beta = 1, f = 0.05, \lambda = 0$ and $\omega_0^2 = -1$.

solution of $x(t)$ of Eq.(3.1), we have calculated Q_s and Q_c from the equation

$$Q_s = \frac{2}{nT}\int_0^{nT} x(t)\sin(\omega t)dt \tag{3.10a}$$

$$Q_c = \frac{2}{nT}\int_0^{nT} x(t)\cos(\omega t)dt \tag{3.10b}$$

with $T = 2\pi/\omega$ is the period of the response and n is taken as 200. Then,

$$Q = \frac{\sqrt{Q_s^2 + Q_c^2}}{f} \tag{3.11}$$

Numerically calculated Q agrees well with the theoretical approximation. In Fig.3(a), for $m_0 = 0.5, 1.0$ and 1.4 the response amplitude Q is found to be maximum at $g = 85.4, 225$ and 425. In Fig.3(b) for $\omega = 0.75.2.5$ and 3.0, resonance is found at $g = 75, 185$ and 255. In Fig.3(c), for $\Omega = 7.5, 21$ and 30 the response amplitude Q is found to be maximum at $g = 38, 150$ and 300. Figure 4(a) shows the phase portrait of slow motion for few values of g around the resonance occurs at $m_0 = 0.5$ with $\lambda = 0, \omega = 1.5$ and $\Omega = 15$ (Fig.3(a)). For $g > g_{VR} = 85.4$ the slow motion oscillation takes place around the origin while for other values of g the center of the orbit moves towards the origin as g increases g_{VR}. Figures 4(b-d) show the actual motion of the system at the resonance occurred at $m_0 = 0.5$ with $\lambda = 0, \omega = 1.5$ and $\Omega = 15$.

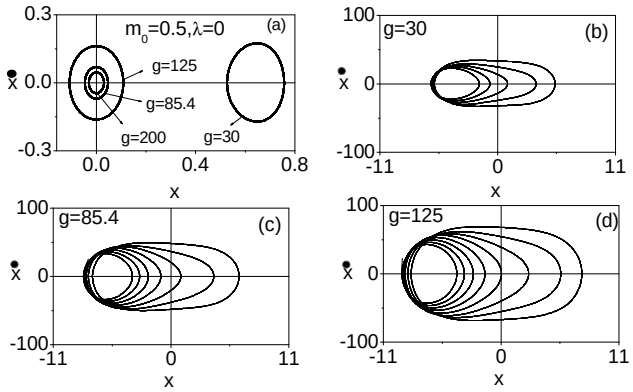

FIGURE 4. Phase portraits of (a) slow motion and (b-d) actual motion of the system with one high-frequency force. The values of the other parameters are $\alpha = 0.2, \beta = 1, f = 0.05, \lambda = 0$ and $\omega_0^2 = -1$.

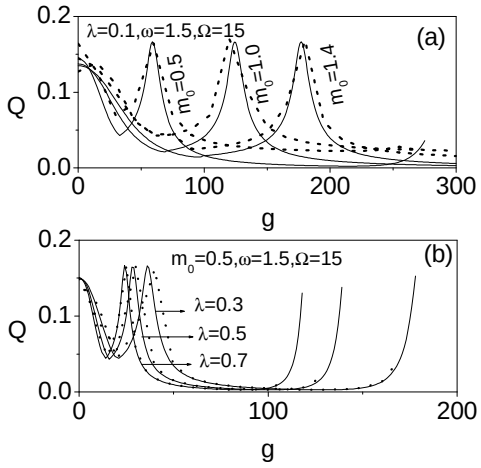

FIGURE 5. The variation of the response amplitude Q (a) with three values of $m_0 = 0.5, 1.0, 1.4$ for $\omega = 1.5, \Omega = 15.0, \lambda = 0.1$ and (b) with three values of $\lambda = 0.3, 0.5, 0.7$ for $m_0 = 0.5, \omega = 1.5, \Omega = 15.0$. The values of the other parameters are $\alpha = 0.2, \beta = 1, f = 0.05$ and $\omega_0^2 = -1$.

From figs.4(b-d), we observed that as g increases, the width and size of the orbit also increases.

Figure 5(a) shows the dependence of the response amplitude Q on g for three values of $m_0 (= 0.5, 1.0, 1.4)$ with $\lambda = 0.1, \omega = 1.5$ and $\Omega = 15.0$. Resonance with single peaks can be clearly seen for each value of m_0. Although resonances can be achieved by varying m_0, there is no significant enhancement in the effect of m_0 on Q, which is a shift in the peak position in the direction of increasing g. In addition, by examining the dependence of Q on g for increasing mass nonlinearity $\lambda = (0.3, 0.5, 0.7)$ at $m_0 = 0.5, \omega = 1.5$ and $\Omega = 15.0$, single resonance peaks are observed for each value of λ. After activating the mass nonlinearity parameter λ, resonances occur earlier than the constant mass (ie., $\lambda = 0$) as can be seen in the Figs.3 and 5.

4. **PDM-Duffing Oscillator with Two High-Frequency Forces**

In the preceding section, we showed that the VR phenomenon can occur in the system with one low- and one high-frequency forces. Next we proceed to verify the existence of VR phenomenon in double-well system driven by an AM force, that is, for the system governed by the Eq.(2.8). The theoretical value of Q is found to be highly different from numerically computed Q. So the analytical expression of Q for the case of system with one high-frequency force is now not applicable for the case of the system with two high-frequency forces. Hence, we numerically integrate the Eq.(2.8) with two high-frequency forces.

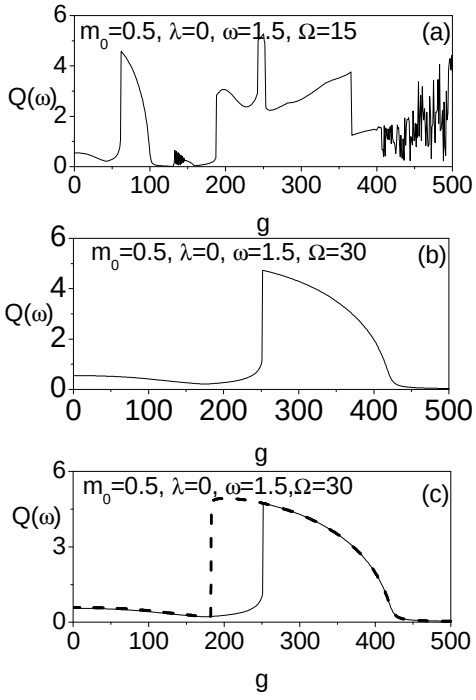

FIGURE 6. Response amplitude Q curves for (a) $\Omega = 15$ (b) $\Omega = 30$ and (c) $Q(\omega)$ obtained by varying the control parameter g from 0 to 500 (continuous curve) and from 500 to 0 (dashed curve) for the PDM-Duffing oscillator with AM force. Other parameters values are $\omega_0^2 = -1, \beta = 1, d = 0.2, m_0 = 0.5, \lambda = 0.0, \omega = 1.5$ and $f = 0.05$.

First we examine the existence of VR phenomenon in the system with constant mass (ie., $\lambda = 0$). The possibility of occurrence of VR through the variation of the mass amplitude m_0 with the high-frequency amplitude g is confirmed by the results presented in Fig.6 for two values of frequency Ω of the high-frequency component of the AM force. Fig.6(a) presents the numerically computed response amplitude Q versus g for $\Omega = 15.0$. When $g < 125.25$ single resonance is obtained and $Q(\omega)$ does not decrease continuously beyond the first resonance peak. $Q(\omega)$ is maximum at more than one value of g and dense resonance peaks are observed in the regions $140.5 < g <$

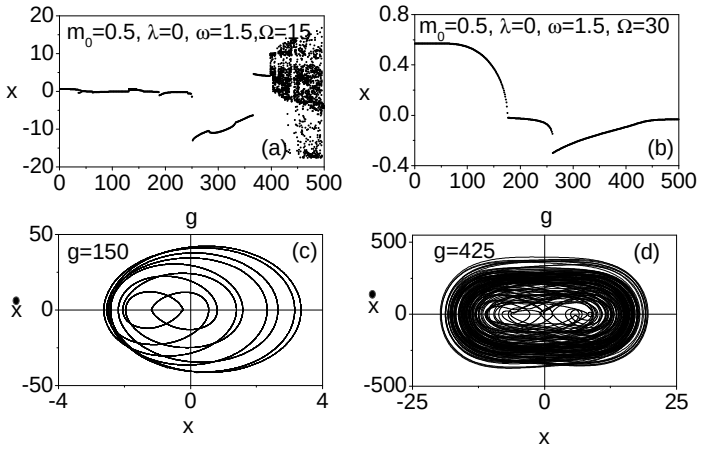

FIGURE 7. Bifurcation diagrams of the double-well PDM-Duffing oscillator driven by an AM force for (a) $\Omega = 15$ and (b) $\Omega = 30$. Phase portraits of the system (c) periodic attractor and (d) chaotic attractor. The parameters values of the system are as in Fig.6 and 6(b).

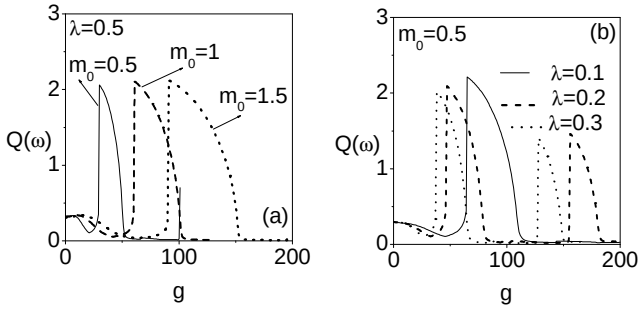

FIGURE 8. The variation of the response amplitude Q with g for three values of (a) mass amplitude m_0 with $\lambda = 0.5$ and (b) mass spatial nonlinearity λ with $m_0 = 0.5$. Other parameters values of the system are fixed as $\omega_0^2 = -1, \beta = 1, d = 0.2, f = 0.05, \omega = 1.5$ and $\Omega = 30.0$.

151.2 and $402.15 < g < 500$. For $\Omega = 30$, $Q(\omega)$ decays to zero as g increases beyond g_{VR} (at which resonance occurs) which is clearly shown in Fig.6(b). Here only one resonance peak is possible. Hysteresis and a jump phenomenon are found in response amplitude curves when g varies in forward and reverse directions. In Fig.6(c), Q is found to follow different paths as indicated by dashed lines where g is varied in the forward and reverse directions. Next we analyze the bifurcation structures of the system (Eq.2.8) for the two values of $\Omega(= 15, 30)$ and the corresponding bifurcation patterns is presented in Fig.7. The other parameters values of the system are as in Fig.6. In Fig.7(a), for increasing values of g, the periodic orbit dominates the dynamics in the high-frequency regime $0 < g < 402.5$ from which the value of g was chosen. For larger values of g, small periodic windows are sandwiched by chaotic regimes . The bifurcation pattern for $\Omega = 30$ is shown in Fig.7(b). For this case, only periodic states appear in the system which is clearly shown in Fig.7(b). For clarity

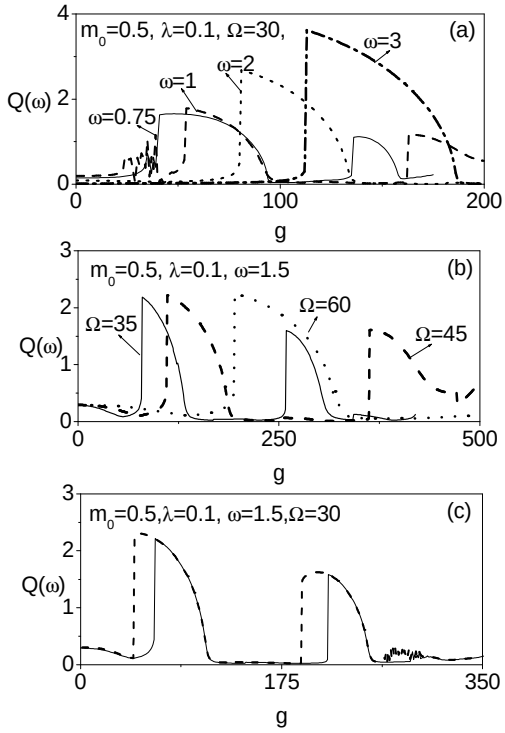

FIGURE 9. Variation of the response amplitude Q with g of the system (Eq.2.8) for (a) four values of ω with $\Omega = 30$ and (b) three values of Ω with $\omega = 1.5$. (c) $Q(\omega)$ is obtained by varying the control parameter g from 0 to 350 (continuous curve) and from 350 to 0 (dashed curve) for the system (Eq.2.8). Other parameters values of the system are fixed as $\omega_0^2 = -1, \beta = 1, d = 0.2, m_0 = 0.5, \lambda = 0.1$ and $f = 0.05$.

an example of periodic and chaotic attractor from Fig.7(a) is shown in Figs.7(c) and 7(d).

So far we have investigated the occurrence of VR in the system with constant mass ($\lambda = 0$). Further in order to know the contributions of the mass spatial nonlinearity parameter λ to VR, we also consider the effect of λ on the observed resonances. First we showed that the resonances for $\lambda = 0.5$ which is presented in Fig.8(a) for varying g and three values of $m_0 (= 0.5, 1, 1.5)$ with $\omega = 1.5, \Omega = 30$. It is observed that the Q_{max} is almost the same in all curves. But g_{max} and width of the resonance curve increases with increasing m_0. In Fig.8(b), $Q(\omega)$ is plotted for different values of λ and with $\omega = 1.5, \Omega = 30$. With increasing λ, double peak resonances occur at $\lambda = 0.2$ and 0.3 and single peak resonance at $\lambda = 0.1$, Q_{max} is different for single and double peak resonances and g_{max} (at which Q is maximum) and width of the resonance curve decreases with increasing λ, which is clearly shown in Fig.8(b).

Finally we study the dependence of Q on the frequencies ω and Ω of the driving forces.In Fig.9(a) $Q(g)$ is plotted for different values ω, namely, $\omega = 0.75, 1, 2, 3$ with $\Omega = 30, m_0 = 0.5, \lambda = 0.1$. With increasing ω, Q_{max} increases. Fig.9(a) has double

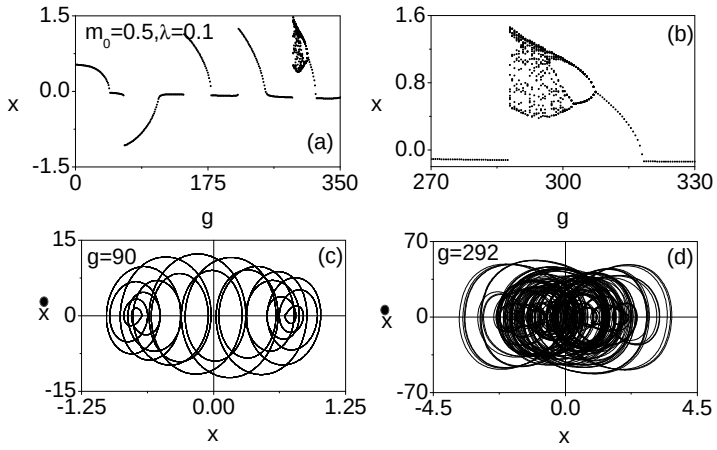

FIGURE 10. Bifurcation diagrams of the PDM-Duffing oscillator driven by an AM force for (a) $m_0 = 0.5, \lambda = 0.1, \omega = 1.5$ and $\Omega = 30$. (b) Magnification of a part of bifurcation diagram in Fig.10(a). Phase portraits of the system (c) periodic attractor and (d) chaotic attractor. The parameters values of the system are as in Fig.9.

peaks for $\omega = 0.75$ and $\omega = 1$ while single peaks for $\omega = 2$ and $\omega = 3$. Width of the resonance curve and g_{max} values increase with increasing ω values. In Fig.9(b) the resonance curve is plotted for three different values of Ω for $\omega = 1.5$ with $m_0 = 0.5$ and $\lambda = 0.1$. Here we again observe that single and double resonances occur for different values of Ω. Q_{max} of the first and second resonances are almost the same in all cases. But g_{max} and width of the resonance curve increases with Ω. The hysteresis and a jump phenomenon in the system is confirmed by Fig.9(c) for $m_0 = 0.5, \lambda = 0.1, \omega = 1.5$ and $\Omega = 30$. Sharp jumps are seen in both Figs.8 and 9. This is caused by nonlinear phenomena such as cyclic fold bifurcation and parameter resonance. For certain cases of the parametric choices, in our study the chaotic motion is found for sufficiently large values of the control parameter g, particularly far after resonance. An example is given in Fig.10(a) for $m_0 = 0.5, \lambda = 0.1, \omega = 1.5$ and $\Omega = 30$. For $0 < g < 330.12$, a period-T solution is found. When g is varied further, reverse period-doubling phenomena leads to chaotic motion, intermittency and periodic windows occur and are clearly shown in Fig.10(b) which is a magnification of a small part of the bifurcation diagram Fig.10(a). For clarity, an example of periodic and chaotic orbits from Fig.10(b) is shown in Figs.10(c) and 10(d).

5. **Conclusion**

In this paper, the VR in a position-dependent mass (PDM)-Duffing oscillator system driven by an amplitude modulated (AM) force is investigated. The amplitude modulated force can be recast into the form $F(t) = f \sin \omega t + g \sin(\Omega + \omega)t + g \sin(\Omega - \omega)t$. We have analyzed and compared the VR in the system induced by one and two

high-frequency forces. Unlike traditional VR theory, VR effects are not only analyzed by signal parameters but also by PDM parameters. The VR phenomenon induced by the two high-frequency forces has certain notable features over the case of only one high-frequency force. Particularly, a higher number of resonance peaks, an enhanced response amplitude Q and non-decaying behaviour of $Q(\omega)$ and hysteresis and a jump phenomenon even for large values of the control parameter g are realized. Our discovery in this paper has potential applications in some fields such as rocket science, tethered satellite dynamics, meteorites, aerology and oceanography. Analysis of VR in the PDM systems with physically interesting forces including frequency modulated force, pulse modulated force and multi external forces may not only give rise to fascinating results but also scope for future research studies

REFERENCES

[1] P.S. Landa and P.V.E. McClintock, Vibrational Resonance, *J. Phys. A*, 33: 1433–1438, 2000.

[2] M. Gitterman, Bistable Oscillator Driven by Two Periodic Fields, *J. Phys.A*, 34: 1355-1357, 2001.

[3] S. Jeyakumari, V. Chinnathambi, S. Rajasekar and M.A.F. Sanjuan, Single and Multiple Vibrational Resonance in a Quintic Oscillator With Monostable Potentials, *Phys. Rev. E*, 80: 046608, 2009.

[4] S. Jeyakumari, V. Chinnathambi, S. Rajasekar and M.A.F. Sanjuan, Analysis of Vibrational Resonance in a Quintic Oscillator, *Chaos*, 19: 043128-8, 2009.

[5] S. Rajasekar, K. Abirami and M.A.F. Sanjuan, Novel Vibrational Resonance in Multistable Systems, *Chaos*, 21(3): 033106, 2011.

[6] U. Ullner, A. Zaikin, J. Garcia-Ojalvo, R. Bascones and J. Kurths, Vibrational Resonance and Vibrational Propagation in Excitable Systems, *Phys. Lett. A*, 312: 348-354. 2003.

[7] H. Yu, J. Wang, C. Liu, B. Deng and X. Wei, Vibrational Resonance in Excitable Neuronal Systems, *Chaos*, 21(4): 043101, 2011 .

[8] B. Deng, J. Wang, X. Wei, K.M. Tsang, and W.L. Chan, Vibrational Resonance in Neuron Populations, *Chaos*, 20: 013117, 2010.

[9] U.E. Vincent, T.O. Roy-Layinde, O.O. Popoola, P.O. Adesina and P.V.E. McClintock, Vibrational Resonance in an Oscillator with an Asymmetrical Deformable Potential, *Phys. Rev. E*, 98(6): 062203, 2018.

[10] T.O. Roy-Layinde, J.A. Laoye, O.O. Popoola and U.E. Vincent, Analysis of Vibrational Resonance in Bi-Harmonically Driven Plasma, *Chaos*, 26(9): 093117, 2016.

[11] J.H. Yang and X.B. Liu, Controlling Vibrational Resonance in a Delayed Multistable System Driven by an Amplitude-Modulated Signal, *Phys. Scr.*, 82(2): 025006, 2010.

[12] A. Daza, A. Wagemakers, S. Rajasekar and M.A.F. Sanjuan, Vibrational Resonance in a Time-Delayed Genetic Toggle Switch, *Commun. Nonlin. Sci. Numer. Simul.*, 18(2): 411-416, 2013.

[13] V.N. Chizhevsky, E. Smeu and G. Giacomelli, Experimental Evidence of Vibrational Resonance in an Optical System, *Phys. Rev. Lett.*, 91(22): 220602, 2003.

[14] V.N. Chizhevsky, Experimental Evidence of Vibrational Resonance in a Multistable System, *Phys. Rev. E*, 89(6): 062914, 2014.

[15] R. Jothimurugan, K. Thamilmaran, S. Rajasekar and M.A.F. Sanjuan, Experimental Evidence for Vibrational Resonance and Enhanced Signal Transmission in Chuas Circuit, *Int. J. Bifur. & Chaos*, 23(11): 1350189, 2013.

[16] K.B. Wolf, *Geometric Optics on Phase Space, Texts and Monographs in Physics*, Springer-Verlag, Berlin, 2004.

[17] J. Awrejcewicz, *Dynamics of Systems of Variable Mass. In Classical Mechanics*, pp.341357. Springer, 2012.

[18] B.G. da Costa and I, Gomez, Information-Theoretical Measures for a Position-Dependent Mass System in an Infinite Potential Well, *Physica A*, 541: 123698, 2000.

[19] S. Cruz y Cruz and O. Rosas-Ortiz, Dynamical Equations, Invariants and Spectrum Generating Algebras of Mechanical Systems with Position-Dependent Mass, *SIGMA*, 9: 004, 2013.

[20] Oscar Rosas-Ortiz, *Position-Dependent Mass Systems: Classical and Quantum Pictures*, arXiv:2002.02297v1 [physics.class-ph] 24th Jan 2020.

[21] C. Quesne and V.M. Tkachuk, Deformed Algebras, Position Dependent Effective Masses and Curved Spaces: An Exactly Solvable Coulomb Problem, *Journal of Physics. A.Mathematical and General*, 37(14): 42674281, 2004.

[22] L. Sierra and E. Lipparini, Spin Response of Unpolarized Quantum Dots, *Europhysics Letters*, 40(6): 667-672, 1997.

[23] F.S.A. Cavalcante, R.N. Costa Filho, J. Ribeiro Filho, C.A.S. de Almeida and V.N. Freire, Form of the Quantum Kinetic energy Operator with Spatially Varying Effective Mass, *Physical Review B*, 55(3): 13261328, 1997.

[24] P.M. Mathews and M. Lakshmanan, On a Unique Nonlinear Oscillator, *Quart.Appl.Math.*, 32: 215-218, 1974.

[25] O. Mustafa, Comment on Nonlinear Dyanmics of a Position Dependent Mass Driven Duffing Oscillator, *J. Phys. A: Math. Theor.*, 46: 032001, 2013.

[26] S.C.Y. Cruz, O. Rosas-Ortiz, Dynamical Equations, Invariants and Spectrum Generating Algebras of Mechanical Systems With Position Dependent Mass, *Symmetry Integr. Feom.*, 9: 4-21, 2013.

[27] T.O. Roy-Layinde, U.E. Vincent, S.A. Abolade, O.O. Popoola, J.A. Laoye and P.V.E. McClintock, Vibrational Resonances in Driven Oscillators with Position-Dependent Mass, *Phil. Trans. R. Soc. A*, 379: 20200227, 2000.

[28] Y. Zhang and S. Li, Combination and Simultaneous Resonances of Gas Bubbles Oscillating in Liquids Under Dual-Frequency Driven Single Bubble in a 6-Dimensional Parameter Space: The Active Cavitation Threshold, *Ultrson.Sonochem.*, 67: 105067, 2007.

[29] I.I. Blekhman and P.S. Landa, Conjugate Resonances and Bifurcations in Nonlinear Systems Under Biharmonical Excitation, *Int. J. Non-Linear Mech.*, 39: 421-426, 2004.